Functionalization and passivation of ultrathin alumina films of defined sub-nanometer thickness with self-assembled monolayers

Zabka, Wolf-Dietrich ; Mosberger, Mathias ; Novotny, Zbynek ; Leuenberger, Dominik ; Mette, Gerson ; Kälin, Thomas ; Probst, Benjamin ; Osterwalder, Jürg

Abstract: Instability of ultrathin surface oxides on alloys under environmental conditions can limit the opportunities for applications of these systems when the thickness control of the insulating oxide film is crucial for device performance. A procedure is developed to directly deposit self-assembled monolayers (SAM) from solvent onto substrates prepared under ultra-high vacuum conditions without exposure to air. As an example, rhenium photosensitizers functionalized with carboxyl linker groups are attached to ultrathin alumina grown on NiAl(1 1 0). The thickness change of the oxide layer during the SAM deposition is quantified by x-ray photoelectron spectroscopy and can be drastically reduced to one atomic layer. The SAM acts as a capping layer, stabilizing the oxide thin film under environmental conditions. Ultraviolet photoelectron spectroscopy elucidates the band alignment in the resulting heterostructure. The method for molecule attachment presented in this manuscript can be extended to a broad class of molecules vulnerable to pyrolysis upon evaporation and presents an elegant method for attaching molecular layers on solid substrates that are sensitive to air.

DOI: https://doi.org/10.1088/1361-648x/aaddd3

Journal of Physics: Condensed Matter

Functionalization and passivation of ultrathin alumina films of defined sub-nanometer thickness with self-assembled monolayers

OPEN ACCESS
IOP Publishing
Journal of Physics: Condensed Matter
J. Phys.: Condens. Matter **30** (2018) 424002 (9pp)
https://doi.org/10.1088/1361-648X/aaddd3

Functionalization and passivation of ultrathin alumina films of defined sub-nanometer thickness with self-assembled monolayers

Wolf-Dietrich Zabka[1], Mathias Mosberger[2], Zbynek Novotny[1], Dominik Leuenberger[1], Gerson Mette[1,3], Thomas Kälin[1], Benjamin Probst[2] and Jürg Osterwalder[1,4]

[1] Department of Physics, University of Zurich, Winterthurerstrasse 190, 8057 Zurich, Switzerland
[2] Department of Chemistry, University of Zurich, Winterthurerstrasse 190, 8057 Zurich, Switzerland

E-mail: osterwal@physik.uzh.ch

Received 21 June 2018, revised 7 August 2018
Accepted for publication 30 August 2018
Published 28 September 2018

Abstract

Instability of ultrathin surface oxides on alloys under environmental conditions can limit the opportunities for applications of these systems when the thickness control of the insulating oxide film is crucial for device performance. A procedure is developed to directly deposit self-assembled monolayers (SAM) from solvent onto substrates prepared under ultra-high vacuum conditions without exposure to air. As an example, rhenium photosensitizers functionalized with carboxyl linker groups are attached to ultrathin alumina grown on NiAl(1 1 0). The thickness change of the oxide layer during the SAM deposition is quantified by x-ray photoelectron spectroscopy and can be drastically reduced to one atomic layer. The SAM acts as a capping layer, stabilizing the oxide thin film under environmental conditions. Ultraviolet photoelectron spectroscopy elucidates the band alignment in the resulting heterostructure. The method for molecule attachment presented in this manuscript can be extended to a broad class of molecules vulnerable to pyrolysis upon evaporation and presents an elegant method for attaching molecular layers on solid substrates that are sensitive to air.

Keywords: self-assembled monolayer, heterostructure, thin film, NiAl, organometallics, surface oxide, photosensitizer

S Supplementary material for this article is available online

(Some figures may appear in colour only in the online journal)

[3] Present address: Fachbereich Physik, Philipps-Universität Marburg, Renthof 5, 35032 Marburg, Germany
[4] Author to whom any correspondence should be addressed.

1. Introduction

Two-dimensional materials and atomic scale engineering allow the fabrication of a new plethora of heterostructures with exciting prospects in fundamental science and application [1–3]. A versatile method to integrate molecular building blocks into functional devices is surface and interface modification with self-assembled monolayers (SAMs) [4, 5]. Numerous applications exist in various fields, e.g. sensor technology [6, 7], electrochemistry [8, 9], catalysis [10], electronic devices [11, 12] and doping of 2D-materials [13–16]. Another surface and interface modification commonly used in heterostructures are insulating ultrathin oxide films of few atomic layer thickness. They attained significant attention as tunnel junctions at interfaces [17–19], and on crystalline metal substrates as model systems for catalysis under ultra-high vacuum (UHV) conditions [20–24]. Controlled oxidation of suitable metallic substrates is a viable approach for the growth of such ultrathin oxide films [21, 25–30]. Unfortunately, not all oxide structures produced under UHV are stable under ambient conditions [31–34]. As a prototypical example, ultrathin alumina films on NiAl alloys are prone to uncontrolled oxidation when exposed to ambient conditions [31–34], thus limiting the scope for applications of ultrathin films with controlled thickness.

In this report, we present a procedure that overcomes this limitation by attaching a dedicated SAM deposition chamber (SAMcham) to our UHV system. It contains two stainless steel bowls that can be filled with the intended SAM solution and with pure solvent for rinsing, and it allows direct transfer to and from UHV without contact to air. As an example, we demonstrate the immobilization of a rhenium tricarbonyl type chromophore containing a 2,2'-bipyridine-4,4'-dicarboxylic acid (DCO_2bipy) for surface binding on a well ordered ultrathin alumina film and characterize it with x-ray photoelectron spectroscopy (XPS). A passivating effect due to the SAM is observed. Moreover, the alignment of molecular levels and substrate bands is measured by ultraviolet photoelectron spectroscopy (UPS).

Ultrathin alumina films on NiAl(1 1 0) are a widely used example for an ultrathin wide gap insulator [21, 22, 24, 36] with well established crystal structure [25, 35]. This surface oxide has a thickness of two atomic bilayers (hence called 2L-alumina from now on; each bilayer contains an aluminum and an oxygen layer) containing oxygen and aluminum atoms in a complex unit cell that forms in two domains and has a $Al_{10}O_{13}$ stoichiometry (see figure 1) [25, 35].

Diimine rhenium(I) tricarbonyl complexes are synthetically versatile photo- and redox-active compounds, which can be incorporated into supramolecular systems, polymers, biomolecules [37–39], and efficient photocatalytic systems for CO_2 reduction [40, 41] as well as H_2 production [42–44]. A derivative of the previously studied *fac*-[Re(NCS)$(CO)_3$(diimine)] (diimine = 2,2'-bipyridine (bipy)) [43, 45, 46] featuring carboxyl linker groups is employed as SAM on the 2L-alumina. Evaporation of such molecules is not feasible, as they are prone to pyrolysis.

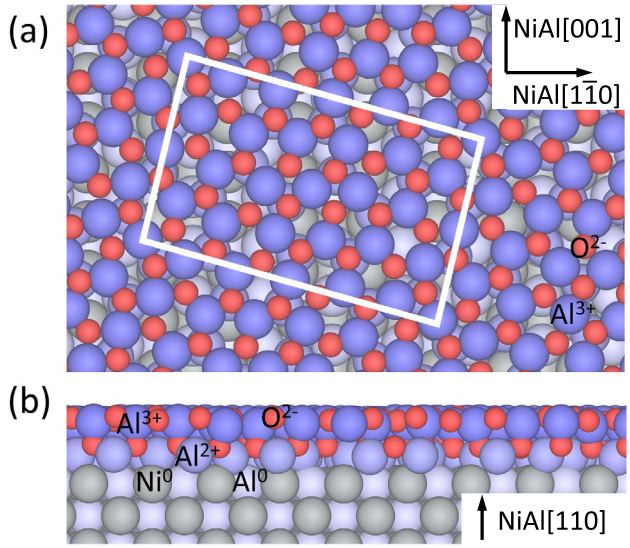

Figure 1. (a) Top and (b) side view of the 2L-alumina/NiAl(1 1 0) according to the structural model of Kresse *et al* [35]. The unit cell of 2L-alumina is marked in white.

2. Results and discussion

The scheme in figure 2(a) shows the structure of the used derivative of *fac*-[Re(NCS)$(CO)_3$(DCO_2bipy)] featuring carboxyl linker groups in the 4 and 4' position of the bipy system and pictures the simplified attachment of the photosensitizer onto the ultrathin oxide film. After the preparation of the 2L-alumina thin films in our UHV system, the sample is brought to the SAMcham while maintaining a high vacuum standard. Two flasks with molecule solution and solvent are connected to the chamber via needles and valves. When the valve between SAMcham and flask is opened, the liquid is pressed inside onto the sample and the vapor pressure is established in the chamber. After this procedure, the solvent is pumped out of the chamber. Figure 2(b) shows the XPS of the Re 4f peak of the clean 2L-alumina (blue), directly after the molecule deposition from acetonitrile (green). Rinsing of the sample removes physisorbed molecules and only the chemisorbed monolayer remains (red). For the multilayer, the intensity of the Re 4f peak is 2.4 times higher. This value gives a lower estimate for the number of layers in the multilayer, neglecting the scattering of photoelectrons within the molecules. After rinsing, the rhenium coverage is (1.29 ± 0.28) atoms nm^{-2}. Considering the dimensions of the molecule, this indicates the formation of a dense monolayer.

Figure 3 shows the (a) Re 4f, (b) S 2p, (c) N 1s, and (d) C 1s core-level spectra of a SAM prepared in this way. For the N 1s peak the difference spectrum using a normalized spectrum of clean 2L-alumina is plotted, as a Ni LMM Auger line occurs in this region with the used Mg Kα x-ray source. The photosensitizer has a chemical formula of $C_{16}H_8N_3O_7ReS$. It contains one rhenium atom in the center, one sulfur atom in the axial thiocyanate ligand and three nitrogen atoms, two of them in the bipy and one in the axial thiocyanate ligand. The binding energies and the stoichiometry of the molecule are summarized in table 1 and refer to data recorded before

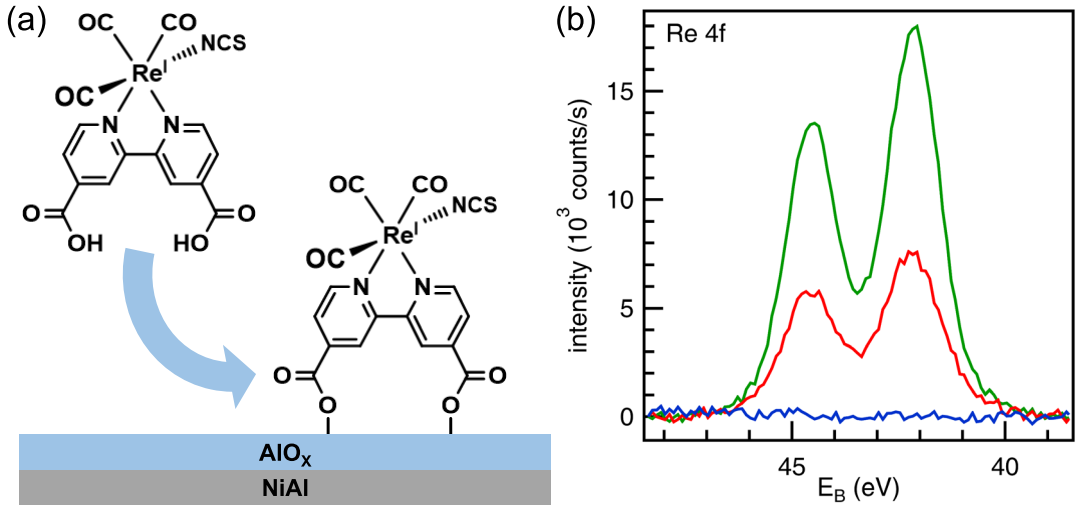

Figure 2. (a) Structure of *fac*-[Re(NCS)(CO)$_3$(DCO$_2$bipy)] featuring two carboxyl linker groups and scheme of molecule anchoring onto the alumina thin film. The carboxyl groups of the molecule bind to the oxide surface. (b) Re 4f core-level spectra before (blue) and after solvent deposition of the photosensitizer (green). After rinsing (red), the chemisorbed monolayer remains on the sample.

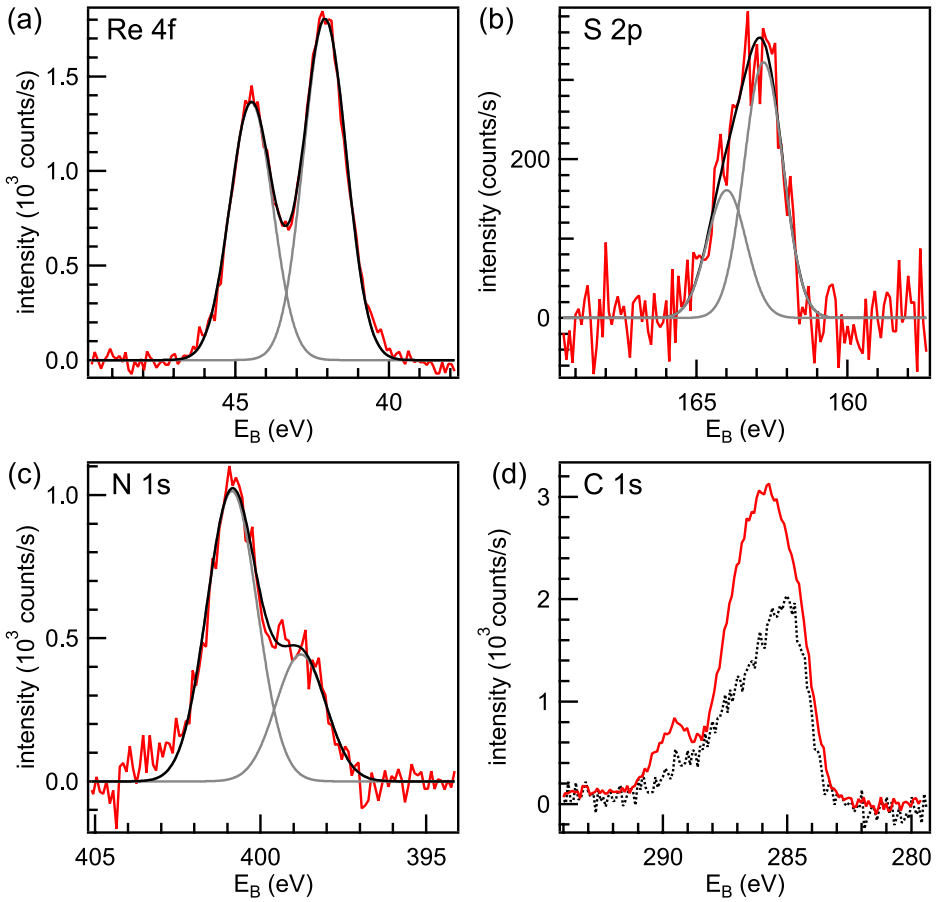

Figure 3. XPS of the SAM (red): (a) Re 4f, (b) S 2p, (c) N 1s (difference spectrum), and (d) C 1s. Fits (black and gray) indicate the spin orbit splitting of the Re 4f and S 2p peaks, and the two components of the N 1s peak. The black dashed line in (d) shows the C 1s contamination which occurs if 2L-alumina is rinsed in acetonitrile without molecules.

radiation damage alters the spectra. Radiation damage of the molecule is observed during the photoemission experiments and discussed in detail in the online supplementary information (see section S1) (stacks.iop.org/JPhysCM/30/424002/mmedia). The stoichiometry of the constituting components is obtained from integrated intensities divided by the respective photoionization cross-sections [47] and is normalized to the Re 4f peak (table 1). The main source for the errors is

attributed to uncertainties in the photoionization cross-sections, which can deviate up to 20% in molecules due to intramolecular inelastic scattering processes and multielectron excitations [48]. An excess of nine carbon atoms is observed, compared to the 16 carbon atoms of the molecule. The dashed black line in figure 3(d) indicates the effect of a preparation with pure solvent, but without molecules (spectrum scaled to the same substrate intensity). Several carbon species are found on the sample when the sample leaves the UHV. Binding energies between 284 and 290 eV are observed, indicating the formation of carbon bonded to oxygen (286–291 eV) and other carbon atoms (285 eV) [49]. Bonding of carbon to aluminum would lead to the formation of carbides (282 eV), which is not observed. We conclude that the observed excess carbon is most likely due to carbon species on the oxygen-terminated alumina surface, but other origins and locations of the remaining carbon cannot be excluded. The binding energy of 162.7 eV of the S $2p_{3/2}$ is in good agreement with the binding energy found for thiocyanate in the N3 dye on 2L-alumina/NiAl(1 1 0) [50], indicating that here similarly the thiocyanate group is not involved in the bonding. Thiocyanate involved in bonding to the substrate delivered in the case of the N3 dye on TiO_2(1 1 0) an additional contribution at 0.7 eV higher binding energies [51]. Also the binding energies found here of 400.9 and 398.8 eV for the nitrogen in the bipy and in the thiocyanate compare well to the binding energies observed in N3/2L-alumina/NiAl(1 1 0) [50]. The carbon peak contains a multitude of contributions due to contamination and a great number of carbon species inside the molecule, however the carboxyl groups at a binding energy of 289.4 eV can unambiguously be identified. In total, these results are consistent with covalent binding of intact molecules to the alumina surface.

Figure 4(a) shows the Shirley background-subtracted Al 2p and Ni 3p spectra of the clean NiAl(1 1 0) substrate (black) with the metallic peaks. The spectra are normalized to the average height of the metallic aluminum peak (Al^0) and the metallic nickel peak (Ni^0). After growing the 2L-alumina film (blue) additional contributions are observed at higher binding energies due to the presence of Al^{2+} in the interfacial oxide layer and Al^{3+} in the second layer (blue) [25, 52]. The shaded area indicates the difference to the bare NiAl(1 1 0) substrate. During SAM deposition with short transfer through air (magenta) a significant intensity increase of oxidized aluminum is observed, corresponding to a thickness of four atomic layers. The shaded area indicates that a significant intensity decrease occurs for the Al^0 peak, and an increase for the Ni^0 peak. This can be explained by a depletion of metallic aluminum at the interface during the oxide formation. As a consequence a higher amount of metallic nickel is left at the interface. These effects can be strongly reduced when SAM deposition is accomplished *in vacuo* (red) in the dedicated SAMcham. Here, the alumina thickness changes only by one atomic layer and the aluminum depletion and nickel enrichment at the interface is significantly reduced.

The reaction of 2L-alumina with water vapor was previously studied by Shavorskiy *et al* [34] using ambient pressure x-ray photoelectron spectroscopy. It was found that relative humidities above 0.01% lead to a drastic increase of the oxide thickness, and to aluminum depletion as well as nickel enrichment in the near surface region. When the SAM deposition is done with a transfer through air (figure 4(a), magenta), a similar change of the surface region is observed. These authors further observed a small thickness increase at a relative humidity of 10^{-5}% associated with surface hydroxylation/oxidation at defect sides of the film present due to reflection and antiphase domain boundaries [53–55]. For straight antiphase domain boundaries an oxygen-deficiency was proven, making them very favorable adsorption sides for new oxygen atoms [55]. In the case with sample transfer through air, the oxygen can originate from the atmosphere. In the case of the *in vacuo* SAM deposition, oxygen might come from the solvent. The molecule attachment can also promote the oxidation of further aluminum atoms: formation of aluminum–oxygen–carbon bonds are a viable scenario during the molecule attachment [56–58]. In the case of hydroxylated alumina surfaces chemisorption of carboxyls will occur via an esterification-like reaction, which releases water molecules [56–59]. Here, the chemisorption of the carboxyl groups on the 2L-alumina surface might also release hydroxyls or water and oxidize the aluminum film further. A shift of the oxygen 1s peak to higher binding energies (see section S2) supports the formation of further oxide or hydroxide.

Table 1. Binding energies measured by XPS, the atomic ratios (obtained from integrated peak intensities and divided by the respective photoionization cross-sections), and comparison to the stoichiometry of the molecule.

Core level	E_B (eV)	Ratio to Re	Expected stoichiometry
Re $4f_{7/2}$	42.1	1.0	1
S $2p_{3/2}$	162.7	0.93 ± 0.19	1
N 1s	400.9	2.3 ± 0.5	2
	398.8	0.99 ± 0.21	1
C 1s	—	25 ± 5	16

Thicker well-ordered alumina films on NiAl(1 1 0) are grown via high-temperature oxidation of 2L-alumina/NiAl(1 1 0) [30]. Figure 4(b) shows the increase of the alumina thickness during the *in vacuo* SAM deposition for sample preparations with different initial alumina thicknesses. For thicker alumina films, the thickness change decreases significantly. Limiting factors for the oxide film thickening could be the rate of charge transfer from the oxide surface to the metal interface [34], the aluminum availability at the interface [34, 60], or the limited mass transport [61]. As no charging was observed during the XPS measurements on these samples and samples with thicker alumina films [30], we exclude the rate of charge transfer as a limiting factor. Further, the aluminium to nickel ratio was the same for samples with different thicknesses [30]. We conclude that the transfer of oxygen and aluminum atoms through thicker oxide films is likely to limit the thickness change.

Figure 5 compares two different samples: one was directly transferred back to the UHV after SAM attachment in the SAMcham (red). For the other sample, the SAM attachment was followed by air exposure for five minutes (black). No significant difference (grey) between both preparations was

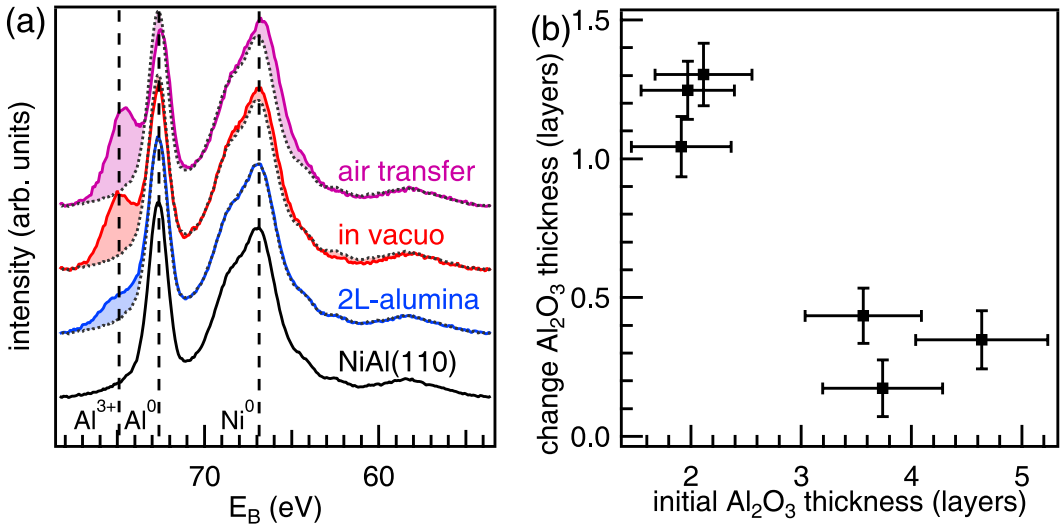

Figure 4. (a) Al 2p and Ni 3p XPS of the NiAl(1 1 0) substrate (black), 2L-alumina (blue), after SAM deposition from solvent on 2L-alumina *in vacuo* (red) and conventional SAM deposition with transfer through air (magenta). The shaded area indicates the change compared to the clean NiAl(1 1 0) substrate (dashed line). (b) Change of the alumina film thickness during *in vacuo* SAM deposition in dependence of the initial oxide film thickness.

detected by means of XPS. Slight changes in the area of the Re 4f peaks of the molecule are due to different stages of radiation damage (see section S1). The intact SAM acts as a capping layer [62, 63], protecting the substrate from further oxidation under ambient conditions. When the molecules are damaged by radiation, this passivation effect is lost (see section S1).

In view of using this molecular system as photoelectrodes, the molecular energy levels and the band alignment in the heterojunction was studied by UPS. Figure 6(a) shows UPS under normal emission of the 2L-alumina/NiAl(1 1 0) substrate (blue), a monolayer (red) and a multilayer (green) coverage of molecules. Two molecular features can be identified in mono- and multilayer samples (multilayer as shown in figure 2(b)). A fit with two Gaussian functions and an exponential background locates the highest occupied molecular orbital (HOMO) in the SAM 2.8 eV beneath the Fermi level. The work function of the SAM is measured using the secondary electron cutoff and decreases as a result of the radiation damage over time. The initial work function is 4.3 eV (see SI: S3).

Figure 6(b) shows the UPS of the different parts of the heterojunction. The metal substrate (black) dictates the position of the Fermi level. As previously determined, the insulating alumina film has a valence band onset 4.2 eV below [30], and a conduction band onset of 2.2 eV above the Fermi level [64]. The observed molecular states appear similarly for the mono- and multilayer coverage, indicating that polarization effects due to the metal substrate are screened and do not alter the electronic structure of the molecule significantly [65, 66]. The same applies for charge transfer between substrate and molecule [19]. We conclude that the electronic structure of the SAM is not influenced drastically by the substrate. Blanco Rodríguez *et al* [45] previously calculated by density functional theory one-electron energies and compositions of relevant molecular orbitals of *fac*-[Re(NCS)(CO)$_3$(bipy)], which

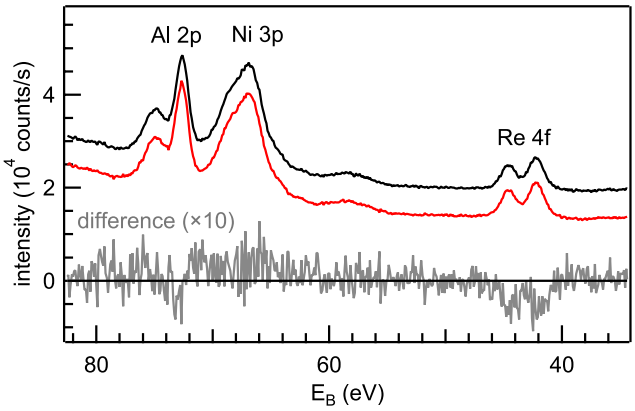

Figure 5. Al 2p, Ni 3p and Re 4f peak after *in vacuo* SAM deposition (red). Air exposure directly after SAM deposition (black, vertical offset) does not alter the heterostructure.

is the core of the molecule used here. These authors concluded that the HOMO and HOMO-1 have a mixed Re/NCS character, are Re-NCS π-antibonding, and are only separated by 50 meV. Distinguishing the HOMO and the HOMO-1 is not possible within the energy resolution of our analyzer and we assign these molecular orbitals to the first observed feature at 2.8 eV beneath the Fermi level. The lowest observed singlet electronic transition for *fac*-[Re(NCS)(CO)$_3$(bipy)] by ultraviolet–visible absorption spectroscopy was reported to be 3.3 eV [45]. For *fac*-[Re(NCS)(CO)$_3$(DCO$_2$bipy)] this transition occurs at 3.0 eV (see section S4), which indicates a 10% smaller gap between the HOMO and the lowest unoccupied molecular orbital (LUMO). This down shift for the optical excitation is likely due to the attached carboxyl groups, which reduces the electron density on the bipy. The LUMO of *fac*-[Re(NCS)(CO)$_3$(bipy)] was calculated by Blanco Rodríguez *et al* [45] to be an antibonding π^* orbital that is mainly located on the bipy at approximately 3.7 eV higher energy. Taking a

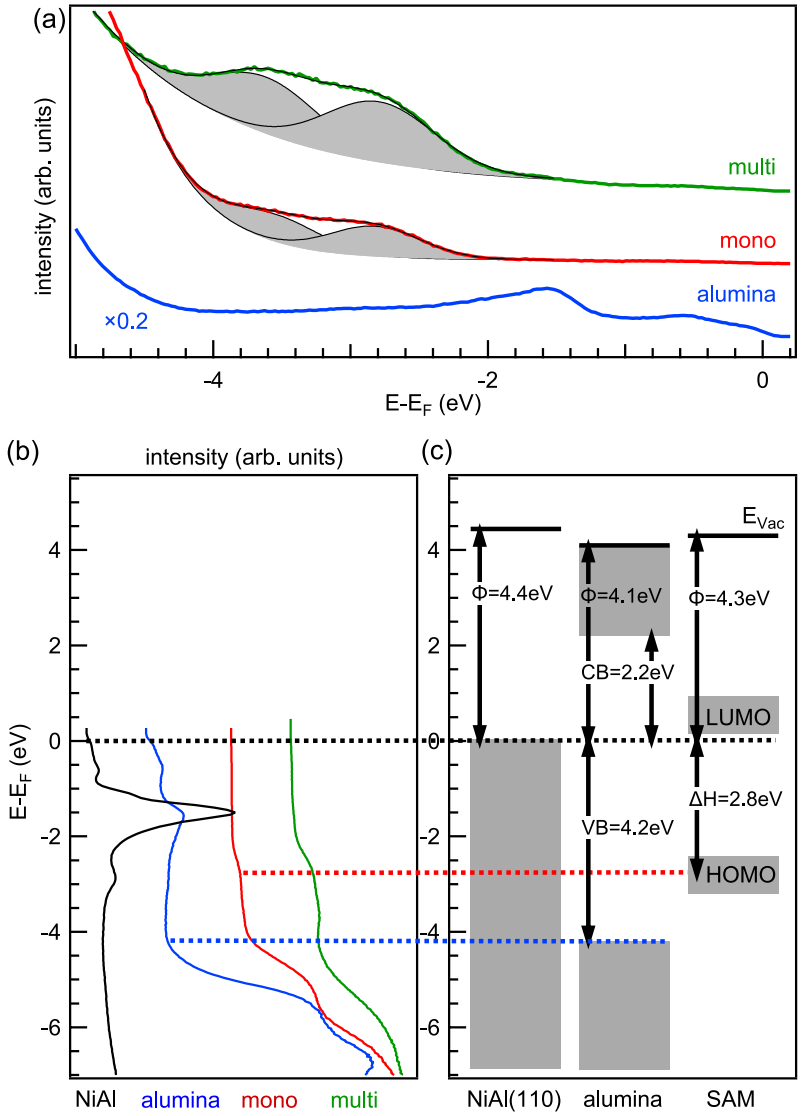

Figure 6. (a) UPS of 2L-alumina, of the SAM (red) and a multilayer (green). Two molecular features are identified with Gaussian fits (gray shaded, exponential background). (b) UPS of NiAl(1 1 0) (black), 2L-alumina (blue), SAM (red) and multilayer (green). (c) The derived band alignment for the multijunction.

10% smaller HOMO–LUMO gap into account, we thus locate the LUMO for *fac*-[Re(NCS)(CO)$_3$(DCO$_2$bipy)] to be 3.3 eV above the HOMO, which is 0.5 eV above the Fermi level. Figure 6(c) summarizes the found electronic band alignment for the metal–insulator–SAM heterostructure. The molecular orbitals are located inside the band gap of the alumina thin film.

3. Summary and outlook

In summary, a method is established for the functionalization and passivation of ultrathin oxide films with SAMs. Exposure of ultrathin oxide films to air leads to a significant increase in thickness of the oxide, which can be reduced to one additional atomic layer of oxide by depositing the SAM in a dedicated chamber *in vacuo*. This enables us to produce a metal–insulator–SAM heterojunction with a precise thickness control of the insulating ultrathin film. The resulting heterostructure is stable in air, making further handling and processing of samples outside of UHV possible without altering of the oxide thin film. The *in vacuo* attachment of SAMs can be extended to a broad class of molecules vulnerable to pyrolysis upon evaporation and presents an elegant method of attaching molecular layers on solid substrates that are sensitive to air. Diimine rhenium(I) tricarbonyl complexes can be incorporated into efficient homogenous photocatalytic systems for CO_2 reduction [40, 41] and H_2 production [42–44], and their attachment as SAM is a step towards their integration into a heterogeneous system. The growth of highly-crystalline alumina films on NiAl(1 1 0) of up to 1.5 nm thickness was previously demonstrated [30]: either cycles of NO_2 adsorption and subsequent annealing [67], or by the high-temperature oxidation of 2L-alumina/NiAl(1 1 0) with oxygen [30] can be used to increase the thickness in a controlled manner. This can enable high-precision tuning of the electron transfer between

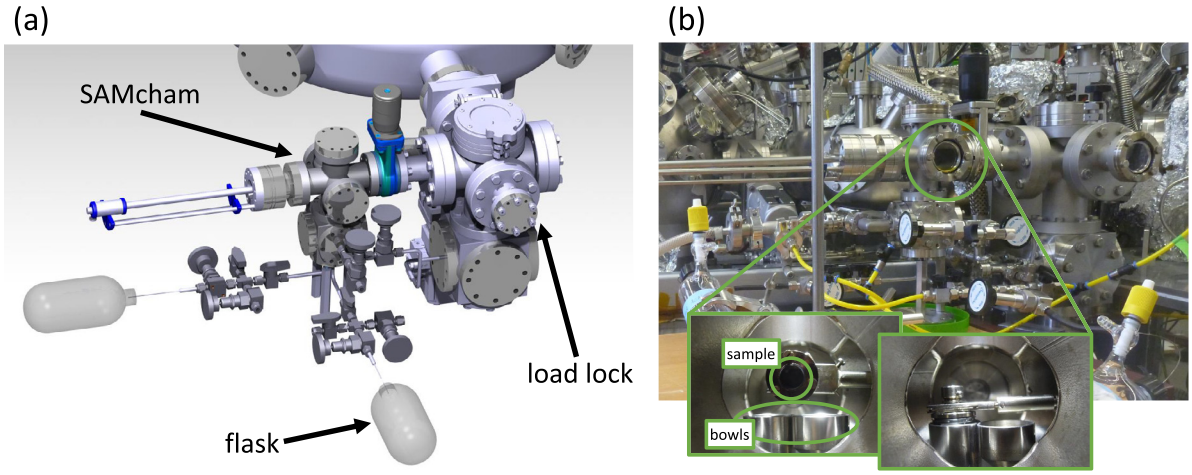

Figure 7. (a) Computer-aided design drawing of the SAMcham. (b) Photograph of the SAMcham. The insets show the inside of the chamber, containing the two bowls for SAM deposition and sample rinsing. A sample is placed with the wobble stick inside the left bowl.

excited molecules and the substrate, as the lifetime of excited charges in the molecule should depend on the thickness of the insulating tunneling layer at the interface.

4. Experimental section

4.1. Oxide thin film preparation

NiAl(1 1 0) single crystals were purchased from MaTecK-Material-Technologie & Kristalle GmbH. The experiments were conducted in a modified VG ESCALAB 220 UHV system with a base pressure of 2×10^{-10} mbar [68]. The NiAl(1 1 0) surface was cleaned with cycles of argon sputtering and subsequent annealing at 1270 K. The 2L-alumina films were prepared by oxidizing the clean NiAl(1 1 0) surface in 5×10^{-6} mbar oxygen at 530 K and subsequent annealing in UHV at 1070 K. The thickness of the thin films was increased systematically by oxidation in 9×10^{-5} mbar oxygen at 970 K, similarly as described in detail by Zabka *et al* [30].

4.2. In vacuo SAM deposition

Similar setups were used previously to transfer samples from UHV to clean electrochemistry environments [69] in order to use single-crystalline samples as electrodes [70, 71]. Here, the samples are similarly transferred from the UHV system via the load lock to the SAMcham (figure 7). The pressure in the SAMcham is in the range of 10^{-6} mbar during the sample transfer. Two flasks are attached via needles to the setup: one with a 0.1 mM solution of the molecule dissolved in acetonitrile for SAM deposition, and one with pure acetonitrile for sample rinsing. The synthesis of the rhenium complex for the SAM is described in the supplementary information (section S5). Acetonitrile (99.9+%, Extra Dry, AcroSeal®) was obtained from *Acros Organics* and additionally degassed by three freeze-pump-thaw cycles. When opening the connecting valves between flask and SAMcham, solvent is pressed into the SAMcham and can splash on the sample. During this procedure the vapor pressure is established in the chamber. After molecule deposition, the chamber is pumped down again and the sample is transferred back into the UHV system. In the first experiments, XPS indicated silicon contamination, which can be avoided by using Teflon-coated septa for the solvent flasks.

4.3. Photoelectron spectroscopy

XPS was conducted at normal emission with an non-monochromatized Mg Kα source, providing photons with an energy of $h\nu = 1253.56$ eV. The energy scale was calibrated as described by Seah [72]. UPS measurements were performed under normal emission with a helium discharge lamp (He I_α, $h\nu = 21.22$ eV).

4.4. Coverage analysis

The coverage of rhenium atoms N_{Re} is calculated by comparing the intensity of the Re 4f peak (I_{Re}) to the intensity of a polycrystalline silver reference sample (I_{Ag}) using equation (1):

$$\begin{aligned} N_{Re} &= \frac{I_{Re}}{\sigma_{Re}} \cdot \frac{\sigma_{Ag}}{I_{Ag}} \cdot \lambda_{Ag} \cdot \cos(\theta) \cdot n_{Ag} \\ &= \frac{I_{Re}}{\sigma_{Re}} \cdot A. \end{aligned} \tag{1}$$

Here, σ_X refers to the corresponding photoionization cross-section [47], θ refers to the electron emission angle with respect to the surface normal, $n_{Ag} = 58.7\ \mathrm{nm}^{-3}$ is the density of silver atoms, and λ_{Ag} is the inelastic mean free path calculated with the Tanuma–Powell–Penn (TPP-2M) equation [73]. The constant A was evaluated for the range of silver peaks from 3s to 4p. The x-ray flux was kept constant.

4.5. Alumina thickness determination

The oxide thickness (d) is calculated numerically by the intensity ratio of the oxidized Al species (I_O) and the metallic Al^0 peak (I_M) according to equation (2):

$$d = \lambda_O \cdot \cos(\theta) \cdot \ln\left[\frac{n_M}{n_O} \cdot \frac{\lambda_M}{\lambda_O} \cdot \frac{I_O}{I_M \exp\left(\frac{d}{\lambda_O \cos(\theta)}\right)} + 1\right] \quad (2)$$

where λ_x refers to the respective inelastic mean free path of the photoelectrons and n_x to the density of Al atoms in the material x ($n_M = 41.6\ \mathrm{nm}^{-3}$, $n_O = 42.7\ \mathrm{nm}^{-3}$, calculated based on structural models from Taylor *et al* [74] and from Smrčok *et al* [75]). $\lambda_O = (2.67 \pm 0.47)$ nm was calculated with the TPP-2M equation. $\lambda_M = (1.99 \pm 0.21)$ nm was normalized by referencing the intensity ratio in the case of 2L-alumina, and is in good agreement with the value obtained with the TPP-2M equation ($\lambda_{M_{\mathrm{TPP-2M}}} = (2.08 \pm 0.43)$ nm). A lattice plane distance of 0.172 nm was used to calculate the number of alumina layers, which is the lattice plane distance of γ-Al_2O_3 in (1 1 1) direction based on structural model from Smrčok *et al* [75]. Equation (2) is similar to the one introduced by Strohmeier [76] for determining the oxide thickness on aluminum alloys, but additionally considers the attenuation of photoelectron intensity from the metal substrate below the oxide in the oxide film.

Acknowledgments

The authors thank Roger Alberto, Thomas Greber, Roland Stania and David Tilley for helpful discussions. This project has been financed under the University Research Priority Program LightChEC of the University of Zurich. MM and BP acknowledge the financial support from the Swiss National Science Foundation SNF (CRSII2_160801/1). GM acknowledges financial support by the Deutsche Forschungsgemeinschaft through SFB 1083 'Structure and Dynamics of Internal Interfaces'.

ORCID iDs

Wolf-Dietrich Zabka https://orcid.org/0000-0002-4949-6495
Dominik Leuenberger https://orcid.org/0000-0002-3318-0533
Gerson Mette https://orcid.org/0000-0001-7561-3264
Benjamin Probst https://orcid.org/0000-0001-8850-9685
Juerg Osterwalder https://orcid.org/0000-0001-9517-641X

References

[1] Barth J V, Costantini G and Kern K 2005 *Nature* **437** 671–9
[2] Mas-Balleste R, Gomez-Navarro C, Gomez-Herrero J and Zamora F 2011 *Nanoscale* **3** 20–30
[3] Novoselov K S, Mishchenko A, Carvalho A and Castro Neto A H 2016 *Science* **353** 9439
[4] Gooding J J and Ciampi S 2011 *Chem. Soc. Rev.* **40** 2704–18
[5] Pujari S P, Scheres L, Marcelis A T M and Zuilhof H 2014 *Angew. Chem. Int. Ed.* **53** 6322–56
[6] Mandler D and Kraus-Ophir S 2011 *J. Solid State Electrochem.* **15** 1535–58
[7] Samanta D and Sarkar A 2011 *Chem. Soc. Rev.* **40** 2567–92
[8] Eckermann A L, Feld D J, Shaw J A and Meade T J 2010 *Coord. Chem. Rev.* **254** 1769–802
[9] Fabre B 2016 *Chem. Rev.* **116** 4808–49
[10] Schoenbaum C A, Schwartz D K and Medlin J W 2014 *Acc. Chem. Res.* **47** 1438–45
[11] Halik M and Hirsch A 2011 *Adv. Mater.* **23** 2689–95
[12] Casalini S, Bortolotti C A, Leonardi F and Biscarini F 2017 *Chem. Soc. Rev.* **46** 40–71
[13] Yan Z, Sun Z, Lu W, Yao J, Zhu Y and Tour J M 2011 *ACS Nano* **5** 1535–40
[14] Hong G, Wu Q H, Ren J, Wang C, Zhang W and Lee S T 2013 *Nano Today* **8** 388–402
[15] Li Y, Xu C Y, Hu P and Zhen L 2013 *ACS Nano* **7** 7795–804
[16] Sim D M, Kim M, Yim S, Choi M J, Choi J, Yoo S and Jung Y S 2015 *ACS Nano* **9** 12115–23
[17] Bibes M, Villegas J E and Barthelemy A 2011 *Adv. Phys.* **60** 5–84
[18] Steurer W, Repp J, Gross L, Scivetti I, Persson M and Meyer G 2015 *Phys. Rev. Lett.* **114** 036801
[19] Hollerer M, Lüftner D, Hurdax P, Ules T, Soubatch S, Tautz F S, Koller G, Puschnig P, Sterrer M and Ramsey M G 2017 *ACS Nano* **11** 6252–60
[20] Freund H J 2010 *Chem. Eur. J.* **16** 9384–97
[21] Diebold U, Li S C and Schmid M 2010 *Annu. Rev. Phys. Chem.* **61** 129–48
[22] Freund H J, Nilius N, Risse T and Schauermann S 2014 *Phys. Chem. Chem. Phys.* **16** 8148–67
[23] Sauer J and Freund H J 2015 *Catal. Lett.* **145** 109–25
[24] Picone A, Riva M, Brambilla A, Calloni A, Bussetti G, Finazzi M, Ciccacci F and Duó L 2016 *Surf. Sci. Rep.* **71** 32–76
[25] Jaeger R M, Kuhlenbeck H, Freund H J, Wuttig M, Hoffmann W, Franchy R and Ibach H 1991 *Surf. Sci.* **259** 235–52
[26] Becker C, Kandler J, Raaf H, Linke R, Pelster T, Dräger M, Tanemura M and Wandelt K 1998 *J. Vac. Sci. Technol.* A **16** 1000–5
[27] Maurice V, Despert G, Zanna S, Bacos M P and Marcus P 2004 *Nat. Mater.* **3** 687–91
[28] Shaikhutdinov S and Freund H J 2012 *Annu. Rev. Phys. Chem.* **63** 619–33
[29] Antlanger M, Mayr-Schmölzer W, Pavelec J, Mittendorfer F, Redinger J, Varga P, Diebold U and Schmid M 2012 *Phys. Rev.* B **86** 035451
[30] Zabka W-D, Leuenberger D, Mette G and Osterwalder J 2017 *Phys. Rev.* B **96** 155420
[31] Maurice V, Frémy N and Marcus P 2005 *Surf. Sci.* **581** 88–104
[32] Kelber J, Magtoto N, Vamala C, Jain M, Jennison D and Schultz P 2007 *Surf. Sci.* **601** 3464–71
[33] Kelber J A 2007 *Surf. Sci. Rep.* **62** 271–303
[34] Shavorskiy A, Müller K, Newberg J T, Starr D E and Bluhm H 2014 *J. Phys. Chem.* C **118** 29340–9
[35] Kresse G, Schmid M, Napetschnig E, Shishkin M, Köhler L and Varga P 2005 *Science* **308** 1440–2
[36] Pacchioni G and Valeri S 2012 *Oxide Ultrathin Films: Science and Technology* (New York: Wiley)
[37] Long C 2010 *Photophysics of Organometallics (Topics in Organometallic Chemistry* vol 29) ed A J Lees (Berlin: Springer) pp 159–91
[38] Vlček A Jr 2010 *Photophysics of Organometallics (Topics in Organometallic Chemistry* vol 29) ed A J Lees (Berlin: Springer) pp 73–114
[39] Lo K K-W 2010 *Photophysics of Organometallics (Topics in Organometallic Chemistry* vol 29) ed A J Lees (Berlin: Springer) pp 115–58
[40] Takeda H, Koike K, Inoue H and Ishitani O 2008 *J. Am. Chem. Soc.* **130** 2023–31
[41] Takeda H and Ishitani O 2010 *Coord. Chem. Rev.* **254** 346–54
[42] Probst B, Kolano C, Hamm P and Alberto R 2009 *Inorg. Chem.* **48** 1836–43

[43] Probst B, Rodenberg A, Guttentag M, Hamm P and Alberto R 2010 *Inorg. Chem.* **49** 6453–60
[44] Probst B, Guttentag M, Rodenberg A, Hamm P and Alberto R 2011 *Inorg. Chem.* **50** 3404–12
[45] Blanco Rodríguez A M, Gabrielsson A, Motevalli M, Matousek P, Towrie M, Šebera J, Záliš S and Vlček A 2005 *J. Phys. Chem.* A **109** 5016–25
[46] Kvapilová H, Vlček A, Barone V, Biczysko M and Záliš S 2015 *J. Phys. Chem.* A **119** 10137–46
[47] Scofield J 1976 *J. Electron. Spectrosc. Relat. Phenom.* **8** 129–37
[48] Söderström J *et al* 2012 *Phys. Rev. Lett.* **108** 193005
[49] Moulder J F, Stickle W F, Sobol P E and Bomben K D 1992 *Handbook of X-Ray Photoelectron Spectroscopy: A Reference Book of Standard Spectra for Identification and Interpretation of XPS Data* ed J Chastain and R C King Jr (Chanhassen, MN: Physical Electronics)
[50] Gibson A J, Temperton R H, Handrup K, Weston M, Mayor L C and O'Shea J N 2014 *J. Chem. Phys.* **140** 234708
[51] Mayor L C, Taylor J B, Magnano G, Rienzo A, Satterley C J, O'Shea J N and Schnadt J 2008 *J. Chem. Phys.* **129** 114701
[52] Martin N M *et al* 2011 *Phys. Rev.* B **83** 125417
[53] Libuda J, Winkelmann F, Bäumer M, Freund H J, Bertrams T, Neddermeyer H and Müller K 1994 *Surf. Sci.* **318** 61–73
[54] Kulawik M, Nilius N, Rust H P and Freund H J 2003 *Phys. Rev. Lett.* **91** 256101
[55] Schmid M, Shishkin M, Kresse G, Napetschnig E, Varga P, Kulawik M, Nilius N, Rust H P and Freund H J 2006 *Phys. Rev. Lett.* **97** 046101
[56] Kasprzyk-Hordern B 2004 *Adv. Colloid Interface Sci.* **110** 19–48
[57] Arrouvel C, Diawara B, Costa D and Marcus P 2007 *J. Phys. Chem.* C **111** 18164–73
[58] Bertazzo S and Rezwan K 2010 *Langmuir* **26** 3364–71
[59] Karaman M, Antelmi D and Pashley R 2001 *Colloids Surf.* A **182** 285–98
[60] Zhang Z, Li L and Yang J C 2011 *Acta Mater.* **59** 5905–16
[61] Evertsson J *et al* 2015 *Appl. Surf. Sci.* **349** 826–32
[62] Laibinis P E and Whitesides G M 1992 *J. Am. Chem. Soc.* **114** 9022–8
[63] Jennings G K, Munro J C, Yong T H and Laibinis P E 1998 *Langmuir* **14** 6130–9
[64] Andersson S *et al* 1999 *Surf. Sci.* **442** L964–70
[65] Repp J and Meyer G 2006 *Appl. Phys.* A **85** 399–406
[66] Freysoldt C, Rinke P and Scheffler M 2009 *Phys. Rev. Lett.* **103** 056803
[67] Mom R V, Vermeer J, Frenken J W and Groot I M 2018 *J. Phys. Chem.* B **122** 788–93
[68] Greber T, Raetzo O, Kreutz T J, Schwaller P, Deichmann W, Wetli E and Osterwalder J 1997 *Rev. Sci. Instrum.* **68** 4549–54
[69] Reniers F 2002 *J. Phys. D: Appl. Phys.* **35** R169
[70] Grumelli D, Wurster B, Stepanow S and Kern K 2013 *Nat. Commun.* **4** 2904
[71] Faisal F *et al* 2018 *Nat. Mater.* **17** 592–8
[72] Seah M P 2001 *Surf. Interface Anal.* **31** 721–3
[73] Tanuma S, Powell C J and Penn D R 1994 *Surf. Interface Anal.* **21** 165–76
[74] Taylor A and Doyle N J 1972 *J. Appl. Crystallogr.* **5** 201–9
[75] Smrčok Ľ, Langer V and Křesťan J 2006 *Acta Crystallogr.* **C62** i83–4
[76] Strohmeier B R 1990 *Surf. Interface Anal.* **15** 51–6